

Magnitude of the Hall fields during magnetic reconnection

A. Le¹, J. Egedal¹, W. Daughton², J. F. Drake³, W. Fox¹, N. Katz¹

In situ observation of the Earth's magnetosphere has identified Hall magnetic fields as a key signature of collisionless magnetic reconnection. The inflow portion of the reconnection diffusion region is further characterized by strong electron pressure anisotropy. These two features are tightly linked in a quantitative model, which is verified using fully kinetic simulations. The model predicts the Hall field strength and the maximum electron pressure anisotropy as functions of the upstream ratio of electron fluid and magnetic pressures.

1. Introduction

Magnetic reconnection allows an often violent reconfiguration of magnetic field lines within a plasma. It accompanies diverse phenomena including magnetic substorms in the Earth's magnetosphere, solar flares, coronal mass ejections, and sawtooth crashes and disruptions in tokamaks. In plasmas with negligible collisions, found in the magnetosphere and the solar wind, reconnection involves the decoupling of electrons and ions in the diffusion region. *Sonnerup* [1979] predicted that this leads to the formation of a quadrupolar Hall magnetic field centered on the reconnection region. The Hall field structure has now been observed in spacecraft data and numerical simulation, and it has been measured in laboratory experiments [*Øieroset et al.*, 2002; *Borg et al.*, 2005; *Drake et al.*, 2008; *Daughton et al.*, 2006; *Hesse et al.*, 2008; *Ren et al.*, 2005; *Brown et al.*, 2006]. Despite the fact that the Hall fields are now considered to be a key signature of collisionless reconnection in space data, there has heretofore been no quantitative theory for the strength of the Hall fields.

Recent in situ observation of the Earth's magnetosphere reveals two more characteristic features of the diffusion region: *Chen et al.* [2008] found electron pressure anisotropy in the inflow plasma with $p_{\parallel} > p_{\perp}$ (where directions are with respect to the magnetic field), and *Phan et al.* [2007] observed evidence for an electron outflow jet near the X-line similar to one observed in their simulations. The outflow electrons stream faster than the $\mathbf{E} \times \mathbf{B}$ speed, and the associated current produces the Hall field. In this Letter, we study the inflow electron pressure anisotropy and, using kinetic simulations, relate it directly to the Hall currents and magnetic fields. Our theory predicts the magnitude of the Hall fields and the electron pressure anisotropy based on the upstream β_e , the ratio of electron and magnetic pressures.

¹Plasma Science and Fusion Center and Physics Department, Massachusetts Institute of Technology, Cambridge, Massachusetts, USA.

²Plasma Theory and Applications, Los Alamos National Laboratory, Los Alamos, New Mexico, USA.

³Institute for Research in Electronics and Applied Physics, University of Maryland, College Park, Maryland, USA.

We begin with the pair of equations of state for the parallel and perpendicular electron pressure originally derived by *Le et al.* [2009] for collisionless reconnection with a guide magnetic field. They are based on an approximate solution of the Vlasov equation for well-magnetized electrons in the limit where electrons trapped by magnetic field gradients and parallel electric fields in the inflow region have bounce frequencies that are fast compared to the electric and magnetic field evolution time scale. For $\tilde{n} = n/n_{\infty} \approx 1$ and $\tilde{B} = B/B_{\infty} < 1$ (∞ refers to the upstream ambient plasma conditions), the equations of state resemble CGL double-adiabatic scalings for the electrons: the pressure components are approximated by $p_{\parallel}/p_{\infty} \approx \pi\tilde{n}^3/6\tilde{B}^2$ and $p_{\perp}/p_{\infty} \approx \tilde{n}\tilde{B}$. Thus, a pressure anisotropy $p_{\parallel}/p_{\perp} \approx \pi\tilde{n}^2/6\tilde{B}^3$ develops due to heating by the parallel electric field and the adiabatic perpendicular cooling associated with μ conservation as the magnetic field strength decreases.

In anti-parallel reconnection, the initial magnetic field geometry contains a neutral sheet where the field vanishes. During the reconnection process, regions of very weak magnetic field persist around neutral points. In principle, this precludes the use of the above equations of state, which assume the particles are magnetized. We find, however, that the electron pressure anisotropy predicted by the equations of state just outside the neutral sheet, where the electrons are still magnetized, imposes useful relationships between the upstream electron pressure and the Hall magnetic fields.

2. Kinetic simulation results

To explore the application of the equations of state to anti-parallel reconnection, we use fully kinetic particle-in-cell (PIC) simulations to study the diffusion region around an X-type neutral point. Fig. 1 shows results from one such simulation. The PIC code is translationally symmetric in the z -direction, has a total domain of 2560×2560 cells = $400d_e \times 400d_e$, and tracks roughly 2×10^9 particles. The initial state is a Harris neutral sheet with gradients in the y direction and is characterized by the following parameters: $m_i/m_e = 400$, $T_i/T_e = 5$, $\omega_{pe}/\omega_{ce} = 2$, and background density = $0.3 n_0$ (peak Harris density). Magnetic reconnection with a single X-line evolves from a small perturbation, and we consider a time with approximately steady-state reconnection.

The density n is fairly uniform in the vicinity of the X-line, while the value of B becomes very low (Fig. 1(a,b)). The quadrupolar out-of-plane Hall magnetic field B_z is shown in Fig. 1(c). We focus on the inner electron diffusion layer where strong electron currents j_z and j_x (Fig. 1(d,e)) flow in a narrow channel. The parallel electric field, plotted in Fig. 1(f), is roughly an order of magnitude smaller than the perpendicular electric field. Even so, the acceleration potential, defined by *Egedal et al.* [2009a] as $\Phi_{\parallel}(\mathbf{x}) = \int_{\mathbf{x}}^{\infty} \mathbf{E} \cdot d\mathbf{l}$ with the integral taken along the magnetic field from the point \mathbf{x} to the ambient plasma where $\mathbf{E} \cdot \mathbf{B} = 0$, becomes roughly as large as the electrostatic potential Φ in Fig. 1(g). The electrostatic potential Φ is negative throughout the outflow region, consistent with Cluster perpendicular electric field measurements reported by *Wygant et al.* [2005]. On the other hand, the acceleration potential Φ_{\parallel} contains a contribution from the out-of-plane inductive reconnection electric field E_z . As visible in Fig. 1(h), Φ_{\parallel} is therefore positive, reaching nearly $\Phi_{\parallel} \sim 4T_e/e$, and it traps a large fraction of the inflow electrons.

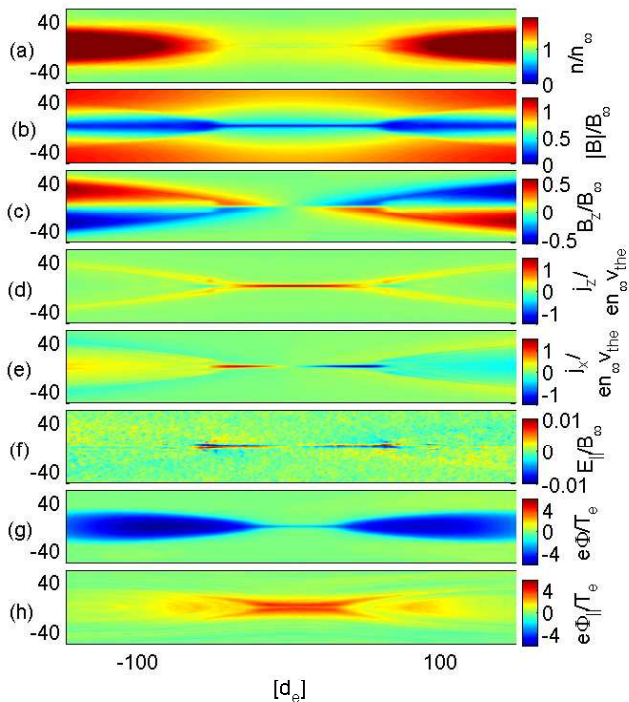


Figure 1. PIC simulation results: (a) plasma density, (b) magnetic field strength, (c), out-of-plane Hall magnetic field B_z , (d) z -directed electron current, (e) x -directed electron current, (f) parallel electric field $\mathbf{E} \cdot \mathbf{B}/B$, (g) electrostatic potential, and (h) acceleration potential.

As stated above, the equations of state apply to the inflow region where the electrons are magnetized. They agree with the PIC simulation to within $\sim 10\%$ up to a layer a few $d_e = c/\omega_{pe}$ wide, where the full electron pressure tensor P_{ij} is used to define $p_{\perp} = \frac{1}{2} [P_{ij} (\delta_{ij} - b_i b_j)]$. The pressure anisotropy in the inflow region is substantial: for the present simulation, the maximum upstream pressure ratio is almost $p_{\parallel}/p_{\perp} \sim 7$ (Fig. 2(a)) Fig. 2(b) shows the PIC pressure anisotropy p_{\parallel}/p_{\perp} divided by the fluid model estimates to illustrate their agreement in the inflow region. In the outflow layer (the rectangular outlines in Figs. 2(a,c)), where

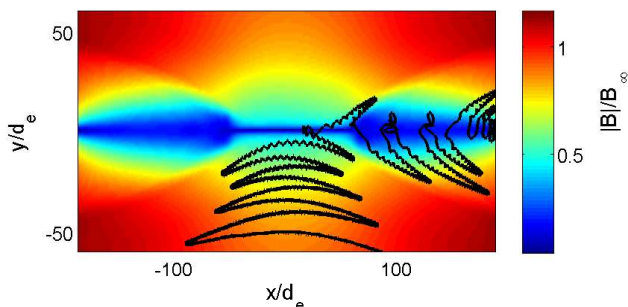


Figure 3. Typical trajectory of a trapped electron overlaid on contours of constant $|\mathbf{B}|$. In the outflow, the electron repeatedly crosses a region of weak magnetic field where μ is not conserved.

the equations of state are inapplicable, the pressure becomes nearly isotropic because the electrons are effectively pitch-angle scattered by passing through the very weak magnetic field. A typical trapped electron trajectory, as shown in Fig. 3(a), crosses the region of weak magnetic field repeatedly as it moves through the outflow region. As noted by *Chen et al.* [2008], strong electron pressure anisotropy may therefore help identify the inflow region in space data.

3. Electron momentum balance

The strong pressure anisotropy predicted by the equations of state affects electron momentum balance in the inner electron diffusion region. Here, the electrons carry almost all of the current (more than 90% throughout the region) and correspondingly nearly all of the $\mathbf{J} \times \mathbf{B}$ force exerted by the magnetic field on the plasma. We highlight the pressure anisotropy by writing steady-state electron momentum balance, assuming $-ne\mathbf{u}_e = \mathbf{J} = \nabla \times \mathbf{B}$, in the form

$$0 = \nabla_i [(B^2/2 + p_{\perp})\delta_{ij} + (p_{\parallel} - p_{\perp} - B^2)b_i b_j] + F_i, \quad (1)$$

where F_i contains the electric field, non-gyrotropic pressure, and inertia contributions. Due to the substantial current in the electron jets, the magnetic field lines are strongly curved and $\nabla_i b_i b_j$ is large. In the PIC simulation, the magnetic tension force across the layer associated with the bent field lines, indicated schematically in Fig. 2(d), is largely balanced by the anisotropic electron pressure, such that just outside the jets $(p_{\parallel} - p_{\perp} - B^2) \approx 0$.

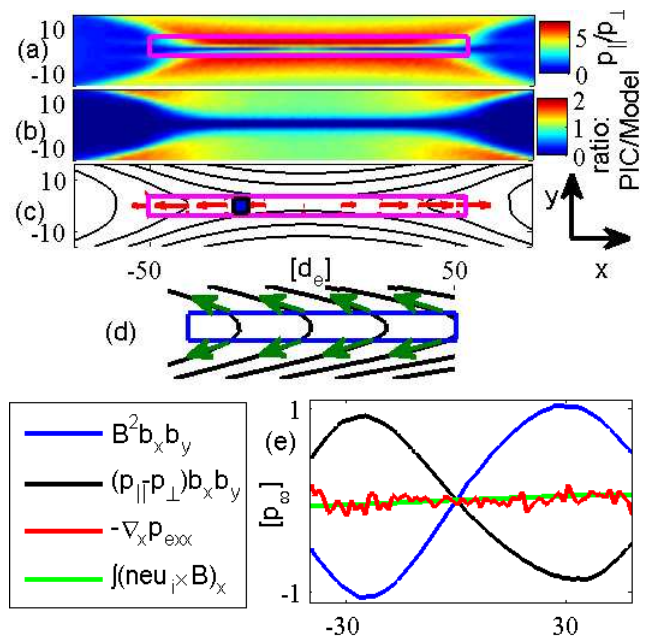


Figure 2. (a) Ratio p_{\parallel}/p_{\perp} from PIC code. (b) Ratio of PIC results and fluid model prediction for p_{\parallel}/p_{\perp} . (The value 1 represents exact agreement.) (c) In-plane projection of magnetic field lines (black) with in-plane electron flow vectors (red). The large magenta rectangle is the electron outflow layer with width $\sim 4d_e$. (d) Magnetic field lines and their tension force. (e) Terms in the integrated momentum balance equation (for an electron fluid element similar to the shaded box in (c) of width $\sim 4d_e$). The magnetic force on the ions (green) is neglected when assuming $\mathbf{J} \sim -ne\mathbf{u}_e$ in the electron outflow layer.

We consider x -momentum balance for differentially narrow fluid elements extending $\sim 4d_e$ across the outflow jet (for example, the small shaded box in Fig. 2(c)). Eq. 1 is integrated over the electron layer using the divergence theorem for the terms in brackets. The largest contributions come from $B^2 b_x b_y$ and $(p_{\parallel} - p_{\perp}) b_x b_y$ evaluated immediately outside the jet and are plotted in Fig. 2(e). A smaller contribution is shown from x gradients in the stress tensor integrated across the layer. The other electron terms that are not plotted are a similar size or smaller. Finally, the integrated magnetic force on the ions is plotted. It is small, and we neglect it when we assume $\mathbf{J} = -ne\mathbf{u}_e$. The terms neglected here become important where the flows peak and then terminate roughly $40d_e$ downstream from the X-line.

Thus, although the electrons acquire a significant outflow velocity within the jets, it is clear from Fig. 2(e) that the tension portion of the $\mathbf{J} \times \mathbf{B}$ force due to $B^2 b_i b_j$ (sketched in Fig. 2(d)) is much greater than the force required to accelerate the electrons. The magnetic tension force is balanced mostly by the anisotropic electron pressure, consistent with previous simulations by Drake *et al.* [2008], and the relevant outside terms approximately cancel: $p_{\parallel} - p_{\perp} \approx B^2$.

4. Predicted scalings

Together with the equations of state $p_{\parallel}(n, B)$ and $p_{\perp}(n, B)$, the main result from force balance considerations, $p_{\parallel} - p_{\perp} \approx B^2$ all along the electron layer, determines parameters of electron diffusion region. Fig. 4 shows $p_{\parallel} - p_{\perp}$ and B^2 as functions of y along a typical cut $15d_e$ to the right of the X-line using both the simulation data and our equations of state. By solving $p_{\parallel}(n, B) - p_{\perp}(n, B) = B^2$ (where the two dashed lines in Fig. 4 intersect), we find the value of the magnetic field strength immediately outside the electron jet, which we denote by B_H .

Taking the density as approximately uniform with $n \approx n_{\infty}$, we obtain B_H as a function only of the ratio of electron to magnetic pressure at the inflow boundary, $\beta_{e\infty} = 2pe_{\infty}/B_{\infty}^2$. This relation is shown in Fig. 4(b). Based on asymptotic limits of the equations of state derived by Le *et al.* [2009], an approximate form valid for small $\beta_{e\infty}$ is

$$\frac{B_H}{B_{\infty}} \approx \left(\frac{\pi \tilde{n}^3 \beta_{e\infty}}{12} \right)^{1/4}. \quad (2)$$

The above scaling is confirmed by three PIC simulations of reconnecting current sheets, each having a mass ratio of $m_i/m_e = 400$, but with varying electron $\beta_{e\infty}$. B_H is evaluated where the out-of-plane electron current reaches 40% of its maximum (roughly $(2 - 4)d_e$ from the peak) and is marked in Fig. 4(b) for the three numerical studies. The middle simulation used fully periodic boundary conditions on the code P3D [Shay *et al.*, 2007], and the others used open boundary conditions on a different code [Daughton *et al.*, 2006].

The momentum balance constraint $p_{\parallel} - p_{\perp} = B^2$ applies everywhere along the length of the electron outflow jets (as seen in Fig. 2(d)). For a given $\beta_{e\infty}$ and a roughly uniform density equal to its value in the ambient plasma, $\tilde{n} = n/n_{\infty} = 1$, the equations of state predict a unique value of B_H that satisfies the momentum balance condition. This implies another result consistent with the simulations: the magnetic field strength is nearly uniform along the current sheet. Although its magnitude is roughly constant and equal to the fixed value $B = B_H$ the magnetic field direction may rotate along the outflow. The component rotated out of the plane is the Hall field B_z . The value of B_H determined from our equations of state outside the current layer is therefore an upper bound for $|B_z|$ in inner diffusion region.

Similarly, the equations of state provide an estimate for the maximum electron pressure ratio p_{\parallel}/p_{\perp} . As visible in Fig. 4(a), the equations of state break down slightly before B reaches the predicted value of B_H . We find empirically from the PIC codes, however, that evaluating the equations of state $p_{\parallel}(n, B)$ and $p_{\perp}(n, B)$ at $n = n_{\infty}$ and $B = 1.25B_H$ (which corresponds to a point where the equations of state are still valid) gives a good estimate for the maximum p_{\parallel}/p_{\perp} in agreement with the three simulations. The scaling plotted in Fig. 4(c) is approximately

$$\left(\frac{p_{\parallel}}{p_{\perp}} \right)_{max} \approx \left(\frac{1}{4\tilde{n}\beta_{e\infty}^3} \right)^{1/4}. \quad (3)$$

In Fig. 4(d), we plot the value of Φ_{\parallel} predicted by our model at the point of maximum upstream pressure anisotropy. Note that at low $\beta_{e\infty}$, a large Φ_{\parallel} develops, scaling roughly as

$$\left(\frac{e\Phi_{\parallel}}{T_{e\infty}} \right)_{max} \approx \frac{1}{2} \left[\left(\frac{4\tilde{n}}{\beta_{e\infty}} \right)^{1/4} - \frac{1}{2} \right]^2, \quad (4)$$

and the majority of inflow electrons are trapped. Because β_e is typically low in Earth's magnetotail, electrical trapping in the inflow region is likely a crucial mechanism for creating the upstream electron pressure anisotropy with $p_{\parallel} > p_{\perp}$ observed by both the Cluster and Wind spacecraft near reconnecting current sheets [Chen *et al.*, 2008; Øieroset *et al.*, 2002]. Our model, however, should be generalized for $\beta_{e\infty} < 0.01$ to account for effects of a large $\Phi_{\parallel} > 10T_e/e$. In particular, the underlying distribution function on which the equations of state are based must be modified [Egedal *et al.*, 2009b].

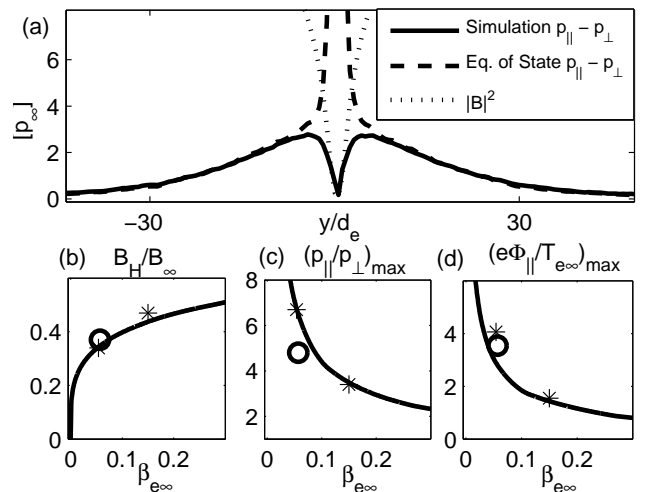


Figure 4. (a) Pressure anisotropy $p_{\parallel} - p_{\perp}$ from PIC simulation and predicted by fluid model, and $|B|^2$. (b-d) Model (curve) compared to PIC simulation results (O, P3D; *, open boundary code) of electron diffusion region parameters depending on ambient electron beta $\beta_{e\infty}$: (b) magnetic field strength B_H just outside outflow layer normalized to reconnecting field B_{∞} , (c) maximum pressure ratio p_{\parallel}/p_{\perp} , and (d) maximum acceleration potential normalized to electron temperature.

5. Summary

Substantial electron pressure anisotropy thus develops in the inflow region during anti-parallel reconnection. The pressure anisotropy is described by equations of state originally derived for guide-field reconnection. The equations of state then link the electron pressure immediately outside the reconnection region to the characteristic strength of the Hall magnetic field B_H through a momentum balance condition, $p_{\parallel} - p_{\perp} \approx B_H^2$, and they set the parameters of the model in terms of the upstream value of β_e . A self-consistent model results in which upstream pressure anisotropy and the curvature of the Hall magnetic field drive perpendicular electron currents beyond the $\mathbf{E} \times \mathbf{B}$ drift speed, and these currents in turn generate the Hall magnetic field.

Acknowledgments. This work was funded at MIT in part by DOE Grant No. DE-FG02-06ER54878 and DOE/NSF Grant No. DE-FG02-03ER54712.

References

- Borg, A. L. et al. (2005), Cluster encounter of a magnetic reconnection diffusion region in the near-Earth magnetotail on September 19, 2003, *Geophys. Res. Lett.*, *12*, L19105, doi:10.1029/2005GL023794.
- Brown, M. R., C. D. Cothran, and J. Fung (2006), Two fluid effects on three-dimensional reconnection in the Swarthmore Spheromak Experiment with comparisons to space data, *Phys. Plasmas*, *13*, 056503, doi:10.1063/1.2180729.
- Chen, L.-J., et al. (2008), Evidence of an extended current sheet and its neighboring magnetic island during magnetotail reconnection, *J. Geophys. Res.*, *113*, A12213, doi:10.1029/2008JA013385.
- Daughton, W., J. Scudder, and H. Karimabadi (2006), Fully kinetic simulations of undriven magnetic reconnection with open boundary conditions, *Phys. Plasmas*, *13*, 072101, doi:10.1063/1.2218817.
- Drake, J. F., M. A. Shay, and M. Swisdak (2008), The Hall fields and fast magnetic reconnection, *Phys. Plasmas*, *15*, 042306, doi:10.1063/1.2901194.
- Egedal, J., W. Daughton, J. F. Drake, N. Katz, A. Le (2009a), Formation of a localized acceleration potential during magnetic reconnection with a guide field, *Phys. Plasmas*, *16*, 050701, doi:10.1063/1.3130732.
- Egedal, J., et al. (2009b), Cluster observations of bi-directional beams caused by electron trapping during anti-parallel reconnection, submitted to *J. Geophys. Res.*
- Hesse, M., S. Zenitani, and A. Klimas (2008), The structure of the electron outflow jet in collisionless magnetic reconnection, *Phys. Plasmas*, *15*, 112102, doi:10.1063/1.3006341.
- Le, A., J. Egedal, W. Daughton, W. Fox, and N. Katz (2009), Equations of state for collisionless guide-field reconnection, *Phys. Rev. Lett.*, *102*, 085001, doi:10.1103/PhysRevLett.102.085001.
- Øieroset, M., R. P. Lin, T. D. Phan, D. E. Larson, and S. D. Bale (2002), Evidence for electron acceleration up to 300 keV in the magnetic reconnection diffusion region of Earth's magnetotail *Phys. Rev. Lett.*, *89*, 195001, doi:10.1103/PhysRevLett.89.195001.
- Phan, T. D., J. F. Drake, M. A. Shay, F. S. Mozer, and J. P. Eastwood (2007), Evidence for an elongated (>60 ion skin depths) electron diffusion region during fast magnetic reconnection, *Phys. Rev. Lett.*, *99*, 255002.
- Ren, Y., et al (2005), Experimental verification of the Hall effect during magnetic reconnection in a laboratory plasma, *Phys. Rev. Lett.*, *95*, 055003.
- Shay, M. A., J. F. Drake, and M. Swisdak (2007), Two-scale structure of the electron dissipation region during collisionless magnetic reconnection, *Phys. Rev. Lett.*, *99*, 155002.
- Sonnerup, B. U. Ö. (1979), Magnetic field reconnection, in *Solar System Plasma Physics*, vol. 3, edited by L. T. Lanzerotti, C. F. Kennel, and E. N. Parker, pp. 45-108, North-Holland, New York.
- Wygant, J. R., et al. (2005), Cluster observations of an intense normal component of the electric field at a thin current sheet in the tail and its role in the shock-like acceleration of the ion fluid into the separatrix region, *J. Geophys. Res.*, *110*, A09206, doi:10.1029/2004JA010708.
- W. Daughton, Plasma Theory and Applications, Los Alamos National Laboratory, X-1-PTA, Los Alamos, NM 97545, USA.
- J. F. Drake, Laboratory for Plasma Research, University of Maryland, Williams Building, College Park, MD 20742, USA.
- J. Egedal, Plasma Science and Fusion Center and Physics Department, Massachusetts Institute of Technology, NW 16-132, 167 Albany Street, Cambridge, MA 02139, USA.
- W. Fox, Plasma Science and Fusion Center, Massachusetts Institute of Technology, NW 16-135, 167 Albany Street, Cambridge, MA 02139, USA.
- N. Katz, Plasma Science and Fusion Center, Massachusetts Institute of Technology, NW 16-133, 167 Albany Street, Cambridge, MA 02139, USA.
- A. Le, Plasma Science and Fusion Center, Massachusetts Institute of Technology, NW 16, 167 Albany Street, Cambridge, MA 02139, USA. (arile@mit.edu)